ELSEVIER

A Reynolds stress closure designed for complex geometries

T. J. Craft and B. E. Launder
Department of Mechanical Engineering, UMIST, Manchester, UK

The paper describes steps in the development of a low Reynolds number second-moment closure for general flow geometries. This requirement means that the model cannot contain geometry-specific quantities, such as the wall-normal vector or wall distance. In their place, invariant dimensionless "gradient indicators" are introduced. New models are also devised for stress dissipation to capture the very diverse behaviour of the different components of ε_{ij} in the wall's vicinity with and without shear. A novel decomposition of the fluctuating pressure terms is also proposed. Applications are shown for shear-free boundary regions, plane channel, and stagnation flows.

Introduction

In recent years computer technology has evolved to a stage where computational fluid dynamics (CFD) can be used to predict a wide range of complex engineering flows. To date, however, the most commonly used turbulence models have been k-ε eddy-viscosity schemes. Yet, second-moment closures offer the potential for far more reliable predictions, since important generation terms are treated exactly. Although these have been shown to be superior in a number of complex flows involving swirl, rotation, buoyancy, etc., the current high Reynolds number versions require modifications before they can be applied to low Reynolds number, near-wall regions. Virtually all current proposals for low Reynolds number models resort to using wall-normal vectors, which makes them inapplicable to complex flow geometries. Some earlier studies (Craft et al. 1993a, b) avoided this problem by employing a simpler eddy-viscosity scheme in the near-wall sublayer; but one of the conclusions to emerge from these was that a better modelling of the near-wall region was required, particularly for accurate heat transfer predictions.

The realizable second-moment closure evolved over several years at UMIST has been found to predict successfully a range of free shear flows (Fu 1988; Craft et al. 1994), and the current work aims to extend this model to be applicable to low Reynolds number regions. This necessitates accounting for effects due to inhomogeneity, strong anisotropy, and the damping of the fluctuating velocity component normal to the wall. One important aspect of the present modelling is that it should be applicable to arbitrary geometries: this means that the "wall-normal" distance and vectors, often included in models, must not be used, since they cannot be uniquely defined for complex surface topographies. Some developments in this direction have been reported by Launder and Tselipidakis (1993) and Launder and Li (1994), who showed that, with suitable inhomogeneity corrections, the above closure could be applied to plane channel flow *without* the need for additional wall-reflection terms. However, experience has shown that this strategy, on its own, is inadequate for handling impinging flows or other situations where the wall region is far from a state of local equilibrium.

Recent direct numerical simulation (DNS) data have proved invaluable in the development of near-wall models, and the present contribution makes particular use of some recent simulations by Perot and Moin (1993) to begin the task of providing a more general strategy for modelling near-wall turbulence. These workers explored the behaviour of decaying turbulence near impermeable boundaries. The studies showed that turbulence does feel significant "wall" effects even in the absence of mean shear. Their simulations included both a shear-free wall (where all velocity components vanish) and an idealized free surface (where only the component normal to the surface vanishes). In this latter flow, the turbulent Reynolds number takes a maximum value at the surface, a feature that helps to distinguish between effects of low turbulent Reynolds number and inhomogeneity.

The remainder of the paper introduces the modelling backgrounds, describes the modelling approaches used for certain processes, and presents results in sheared, impinging, and shear-free flows.

Modelling approach

The Reynolds stress transport equations can be written as

$$\frac{D\overline{u_i u_j}}{Dt} = P_{ij} + \Pi_{ij} - \varepsilon_{ij} + d_{ij} \tag{1}$$

where, in the absence of force fields and significant density variations, the stress production P_{ij} is simply $-(\overline{u_i u_k}\,\partial U_j/\partial x_k + \overline{u_j u_k}\,\partial U_i/\partial x_k)$ and requires no modelling. The diffusion term d_{ij} is given by

$$d_{ij} = \frac{\partial}{\partial x_k}\left(\nu\frac{\partial \overline{u_i u_j}}{\partial x_k} - \overline{u_i u_j u_k}\right) \tag{2}$$

Address reprint requests to Dr. T. J. Craft, Department of Mechanical Engineering, UMIST, P.O. Box 88, Manchester M60, UK.

Received 13 October 1995; accepted 30 January 1996

Int. J. Heat and Fluid Flow 17: 245–254, 1996

655 Avenue of the Americas, New York, NY 10010

0142-727X/96/$15.00
PII S0142-727X(96)00038-4

In the present work, the triple correlation is approximated by the Hanjalic–Launder (1972) proposal:

$$\overline{u_i u_j u_k} = -0.11\frac{k}{\varepsilon}\left[\overline{u_i u_l}\frac{\partial \overline{u_j u_k}}{\partial x_l} + \overline{u_j u_l}\frac{\partial \overline{u_i u_k}}{\partial x_l} + \overline{u_k u_l}\frac{\partial \overline{u_j u_i}}{\partial x_l}\right] \quad (3)$$

The pressure correlation $\Pi_{ij} = -(\overline{u_i\,\partial p/\partial x_j} + \overline{u_i\,\partial p/\partial x_j})/\rho$ is often split into a pressure–strain correlation ϕ_{ij} and a pressure-diffusion term d_{ij}^p, where

$$\phi_{ij} = \overline{\frac{p}{\rho}\left(\frac{\partial u_i}{\partial x_j} + \frac{\partial u_j}{\partial x_i}\right)} \quad \text{and} \quad d_{ij}^p = -\frac{1}{\rho}\left(\frac{\partial \overline{pu_i}}{\partial x_j} + \frac{\partial \overline{pu_j}}{\partial x_i}\right) \quad (4)$$

Lumley (1975) has pointed out, however, that there are various ways of decomposing Π_{ij} into diffusive and redistributive parts; the present work in fact adopts such a nonconventional decomposition.

In the closure developed in later sections, the wall-normal vector is not used, since it limits the applicability of the model to geometrically simple configurations. It is, nevertheless, desirable to have some parameter which identifies the direction in which strong inhomogeneity is present. The current proposals, in fact, adopt not just one but *two* inhomogeneity indicators based on gradients of the turbulent length scale, $l \equiv k^{3/2}/\varepsilon$. While the parameter $N_i \equiv \partial l/\partial x_i$ is dimensionless and has been used in a number of proposals (e.g., Launder and Tselipidakis 1993), for present purposes, it is desirable to normalize N_i so that, in regions of strong inhomogeneity, it is the *direction* of inhomogeneity, rather than the magnitude of the length-scale-gradient itself, that is flagged. However, if the inhomogeneity is only weak, one does not want any appreciable inhomogeneity correction to be applied. These twin objectives are served by adopting for modelling the parameter d_i:

$$d_i \equiv N_i/(\alpha + (N_k N_k)^{1/2}) \quad (5)$$

The quantity α has been taken as 0.5, while, for a local-equilibrium near-wall shear flow, $(N_k N_k)^{1/2}$ takes a value of about 2.5 in the fully turbulent region.

An objection to using N_i is that, in the "buffer region" of a wall shear flow, the length scale $k^{3/2}/\varepsilon$ levels out giving undesirably small levels of d_i in what is a highly inhomogeneous region. This problem is removed by introducing Lumley's (1978) flatness factor A, defined below, so that

$$N_i^A \equiv \frac{\partial}{\partial x_i}(lA) \quad \text{and} \quad d_i^A = \frac{N_i^A}{\alpha + (N_k^A N_k^A)^{1/2}} \quad (6)$$

The parameter A takes the value unity in isotropic turbulence and vanishes at a wall or free surface where the turbulence fluctuations reduce to a two-component form. The strong rise in A across the buffer region ensures substantial levels of N_i^A and thus of d_i^A.

To illustrate this point, Figure 1 shows d_i and d_i^A for the plane channel flow of Kim et al. (1987) evaluated from the DNS data. Evidently the use of d_i^A has removed the problematical minimum that occurs with d_i at $y/h \approx 0.15$ (the channel width being $2h$).

The turbulent Reynolds number R_t is also used to provide some near-wall damping, but its influence is restricted to regions where R_t is less than about 200, since it is generally held that viscous effects should become negligible at higher R_t. The stress invariants $A_2 \equiv a_{ij}a_{ij}$; $A_3 \equiv a_{ij}a_{jk}a_{ki}$ and the flatness parameter A, introduced above, (defined as: $A \equiv 1 - 9/8(A_2 - A_3)$ where $a_{ij} \equiv \overline{u_i u_j}/k - 2/3\delta_{ij}$) are also used, since they enable the model to be sensitized to the anisotropy of the Reynolds stress.

Notation

A	Lumley's "stress flatness" invariant
A_2, A_3	second and third invariants of stress anisotropy
a_{ij}	dimensionless stress anisotropy, $\overline{u_i u_j}/k - 2\delta_{ij}/3$
d_i, d_i^A	indicators of length-scale gradient direction
d_{ij}	diffusive transport of $\overline{u_i u_j}$
d_{ij}^p	diffusive transport of $\overline{u_i u_j}$ due to pressure fluctuations
k	turbulent kinetic energy
L_o	reference length
N_i, N_i^A	length-scale gradient vectors
P_{ij}	stress production tensor
p	pressure fluctuation
Q_{ij}	Perot–Moin tensor: $Q_{pk}Q_{kq} \equiv \overline{u_p u_q}$
R_t	turbulent Reynolds number, $k^2/\nu\varepsilon$
T	mean temperature
T_o	reference time
t	time
u_i	velocity fluctuation
$\overline{u_i u_j}$	kinematic Reynolds stress
u', v', w'	Cartesian components of rms fluctuating velocity
x_j	Cartesian coordinate (normally: x_1 stream direction, x_2 direction of inhomogeneity)
y	coordinate, orthogonal to mean flow in direction of inhomogeneity

Greek

δ_{ij}	Kronecker delta
ε	kinematic dissipation rate of k
$\tilde{\varepsilon}$	homogeneous dissipation rate of k
ε_{ij}	dissipation rate of $\overline{u_i u_j}$
$\varepsilon'_{ij}, \varepsilon''_{ij}, \varepsilon^*_{ij}$	different contributors to ε_{ij} (see Equation 9)
Π_{ij}	pressure-gradient-velocity tensor, $-(\overline{u_i\,\partial p/\partial x_j} + \overline{u_j\,\partial p/\partial x_i})/\rho$
ϕ_{ij}	conventional pressure–strain tensor
ρ	fluid density
τ_w	wall shear stress
ϕ^*_{ij}	modified pressure–strain tensor
$\varphi^*_{ij1}, \phi^*_{ij2}$	turbulence and mean-strain contributions to ϕ^*_{ij}

Superscripts

$+$	quantity nondimensionalized with τ_w, ρ, and ν
$'$	denotes rms value of indicated velocity

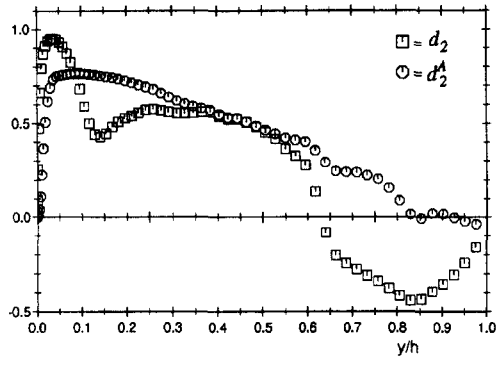

Figure 1 Profiles of d_2 and d_2^A in plane channel flow

Dissipation tensor ε_{ij}

In most high Reynolds number models, the smallest scale dissipative eddies are assumed to be isotropic, so that ε_{ij} is modelled as $2/3\varepsilon\delta_{ij}$. At lower Reynolds numbers it is often supposed that $\varepsilon_{ij} = \varepsilon\overline{u_i u_j}/k$ is a better approximation though, at a solid wall, Launder and Reynolds (1983) showed that the limiting behaviour of ε_{ij} is given by

$$\frac{\varepsilon_{11}}{\overline{u_1^2}} = \frac{\varepsilon_{33}}{\overline{u_3^2}} = \frac{1}{4}\frac{\varepsilon_{22}}{\overline{u_2^2}} = \frac{1}{2}\frac{\varepsilon_{12}}{\overline{u_1 u_2}} = \frac{\varepsilon}{k} \tag{7}$$

However, this limit is not valid at a free surface, since then $\overline{u_2^2} \sim y^2$ and ε_{22} is nonzero at the surface where it balances the molecular diffusion.

Perot and Moin (1993), by postprocessing their DNS data, proposed a model for ε_{ij} which had the very simple near-wall form

$$\varepsilon_{ij} = 2\nu\frac{\partial Q_{ik}}{\partial x_l}\frac{\partial Q_{jk}}{\partial x_l} \tag{8}$$

where the tensor Q_{ij} was defined by $Q_{ik}Q_{kj} = \overline{u_i u_j}$. Unfortunately, this was found to be unsuitable for use in computations. At the wall, the $\overline{u_2^2}$ budget consists of a balance between viscous diffusion and dissipation: the form of Equation 8 is such that this balance is achieved for $\overline{u_2^2} \sim y^n$, for *any* value of n; consequently, the near-wall behaviour simply becomes a function of the initial conditions.

The present work employs the following composite form specifically to address the behaviour of ε_{ij} near walls and free surfaces indicated by the DNS results:

$$\varepsilon_{ij} = \left(1 - f_h\frac{\varepsilon^*_{kk}}{2\varepsilon}\right)\left[(1-f_\varepsilon)(\varepsilon'_{ij} + \varepsilon''_{ij})/D + \frac{2}{3}f_\varepsilon\varepsilon\delta_{ij}\right] + f_h\varepsilon^*_{ij} \tag{9}$$

In Equation 9 the various components take the following forms:

$$\varepsilon'_{ij} = \varepsilon\frac{\overline{u_i u_j}}{k} + 2\nu\frac{\overline{u_l u_n}}{k}\frac{\partial\sqrt{k}}{\partial x_l}\frac{\partial\sqrt{k}}{\partial x_n}\delta_{ij} + 2\nu\frac{\overline{u_l u_i}}{k}\frac{\partial\sqrt{k}}{\partial x_j}\frac{\partial\sqrt{k}}{\partial x_l} + 2\nu\frac{\overline{u_l u_j}}{k}\frac{\partial\sqrt{k}}{\partial x_i}\frac{\partial\sqrt{k}}{\partial x_l}$$

$$\varepsilon''_{ij} = \varepsilon\left[2\frac{\overline{u_l u_k}}{k}d_l^a d_k^a\delta_{ij} - \frac{\overline{u_l u_i}}{k}d_l^a d_j^a - \frac{\overline{u_l u_j}}{k}d_l^a d_i^a\right]f_R$$

$$\varepsilon^*_{ij} = 0.2\nu\left(\frac{\partial\sqrt{kA}}{\partial x_k}\frac{\partial\sqrt{kA}}{\partial x_k}\delta_{ij} + 2\frac{\partial\sqrt{kA}}{\partial x_i}\frac{\partial\sqrt{kA}}{\partial x_j}\right)$$

and where

$$D = (\varepsilon'_{kk} + \varepsilon''_{kk})/(2\varepsilon)$$

$$f_R = (1-A)\min((\mathrm{R}_t/80)^2, 1.0) \qquad f_\varepsilon = A^{1/2}$$

$$f_h = 1 - \exp(-\mathrm{R}_t/50)$$

If we first disregard effects of inhomogeneity, Equation 9 causes the component dissipation to vary between $2/3\varepsilon\delta_{ij}$ and $\varepsilon\overline{u_i u_j}/k$ depending on the magnitude of f_ε, the argument of the latter function being a function of A rather than the more usual R_t. The need for this change of argument is brought out emphatically by considering the low Reynolds number simulations of channel flow: then R_t reaches its maximum value near the edge of the buffer layer whereas the anisotropy of the dissipation, like that of $\overline{u_i u_j}$, decreases all the way to the centre. The term ε'_{ij} is only effective across the viscous sublayer where k-gradients are steep; there it acts to satisfy the limits of Equation 7. The proposed term ε''_{ij} principally has the effect of producing the dip in ε_{12} seen at around $y/\delta = 0.1$ in near-wall DNS studies. This feature has been ignored in earlier near-wall models. The term ε^*_{ij} is designed to improve the behaviour of ε_{ij} at a free surface, where there are significant inhomogeneity effects and the turbulent Reynolds number is high.

Predictions of the dissipation component resulting from this modelling for the cases of a free-surface flow, a shear-free wall, and plane Couette flow are shown in Figure 2. The closure predictions draw on values of $\overline{u_i u_j}$ and ε from the DNS results. The very diverse variations exhibited by the different components across the three flows are captured encouragingly well.

Pressure correlation modelling

In homogeneous flows, the pressure diffusion term is zero, and consequently it is only the pressure–strain term which contributes to the pressure correlation. In near-wall flows, both terms are present, and one question to be addressed is the best way of decomposing the Π_{ij} term. The conventional decomposition is into the pressure–strain and diffusional parts indicated by Equation 4. However, Figure 3 shows the distribution of ϕ_{ij} and the quantity $\phi^*_{ij} = \Pi_{ij} - d^p_{kk}\overline{u_i u_j}/(2k)$ in the three flows considered. Notice that ϕ_{ij} itself shows significant differences between shear-free flows near a wall and a free surface. In contrast, the quantity ϕ^*_{ij} shows the same qualitative behaviour, suggesting that it will be easier to model.

The model currently proposed for ϕ^*_{ij} can be written:

$$\phi^*_{ij} = \phi^*_{ij1} + \phi^*_{ij2} + \phi^{\mathrm{inh}}_{ij1} + \phi^{\mathrm{inh}}_{ij2} \tag{10}$$

where

$$\phi^*_{ij1} = -c_1\tilde{\varepsilon}\left[a_{ij} + c'_1\left(a_{ik}a_{kj} - \frac{1}{3}A_2\delta_{ij}\right)\right] - \tilde{\varepsilon}Aa_{ij}$$

$$\phi^*_{ij2} = -0.6\left(P_{ij} - \frac{1}{3}\delta_{ij}P_{kk}\right) + 0.3a_{ij}P_{kk} - 0.2\left[\frac{\overline{u_k u_j}\,\overline{u_l u_i}}{k}\left[\frac{\partial U_k}{\partial x_l} + \frac{\partial U_l}{\partial x_k}\right] - \frac{\overline{u_l u_k}}{k}\left[\overline{u_i u_k}\frac{\partial U_j}{\partial x_l} + \overline{u_j u_k}\frac{\partial U_i}{\partial x_l}\right]\right]$$

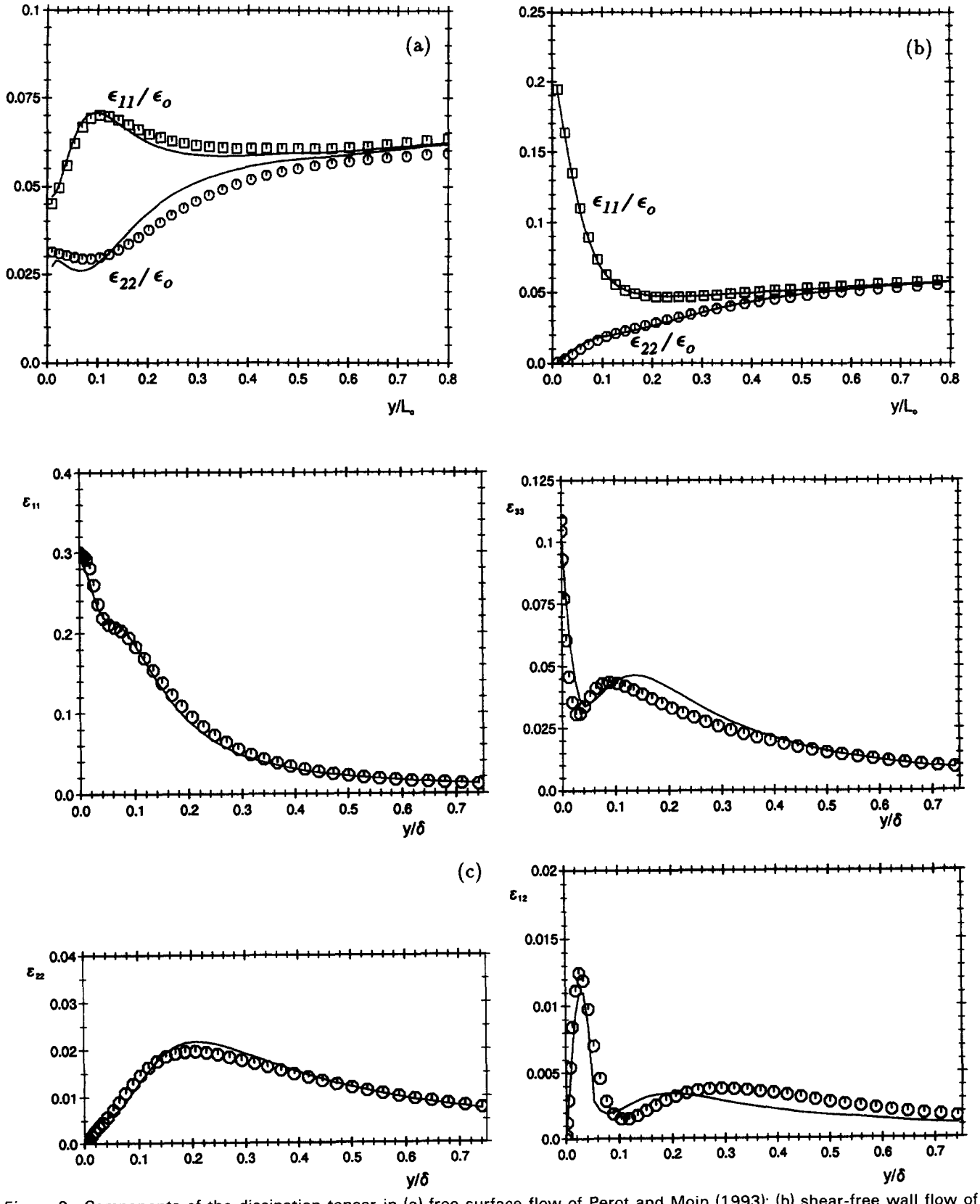

Figure 2 Components of the dissipation tensor in (a) free-surface flow of Perot and Moin (1993); (b) shear-free wall flow of Perot and Moin (1993); and (c) plane Couette flow of Kuroda et al. (1993)

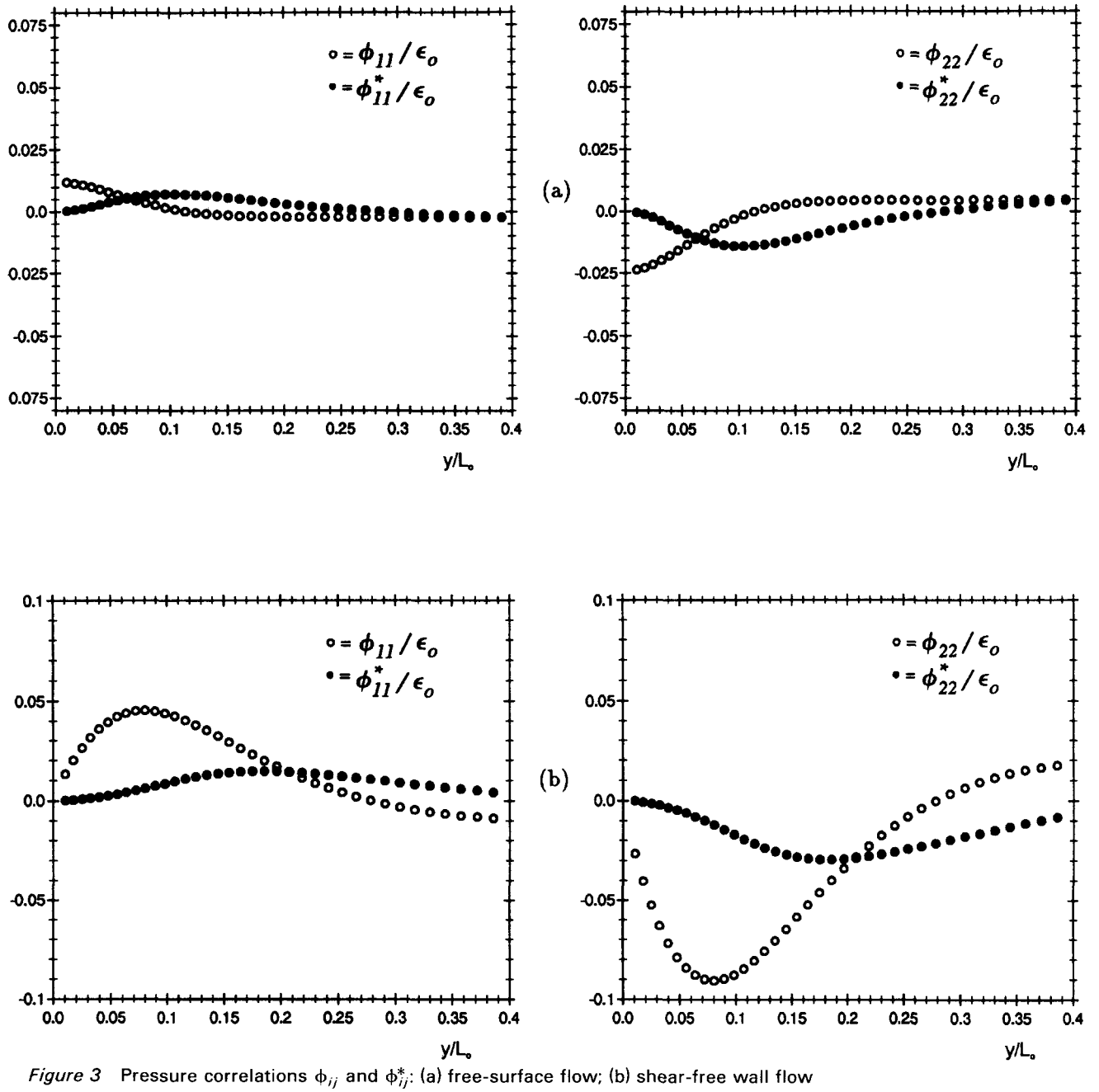

Figure 3 Pressure correlations ϕ_{ij} and ϕ^*_{ij}: (a) free-surface flow; (b) shear-free wall flow

$$
\begin{aligned}
&- c_2[A_2(P_{ij} - D_{ij}) + 3a_{mi}a_{nj}(P_{mn} - D_{mn})] \\
&+ c_2'\left\{\left(\frac{7}{15} - \frac{A_2}{4}\right)\left(P_{ij} - \frac{1}{3}\delta_{ij}P_{kk}\right)\right. \\
&+ 0.1\left[a_{ij} - \frac{1}{2}\left(a_{ik}a_{kj} - \frac{1}{3}\delta_{ij}A_2\right)\right]P_{kk} - 0.05a_{ij}a_{lk}P_{kl} \\
&+ 0.1\left[\left(\frac{\overline{u_iu_m}}{k}P_{mj} + \frac{\overline{u_ju_m}}{k}P_{mi}\right) - \frac{2}{3}\delta_{ij}\frac{\overline{u_lu_m}}{k}P_{ml}\right] \\
&+ 0.1\left[\frac{\overline{u_lu_i}\,\overline{u_ku_j}}{k^2} - \frac{1}{3}\delta_{ij}\frac{\overline{u_lu_m}\,\overline{u_ku_m}}{k^2}\right] \\
&\times\left[6D_{lk} + 13k\left[\frac{\partial U_l}{\partial x_k} + \frac{\partial U_k}{\partial x_l}\right]\right] \\
&\left.+ 0.2\frac{\overline{u_lu_i}\,\overline{u_ku_j}}{k^2}(D_{lk} - P_{lk})\right\}
\end{aligned}
$$

Table 1 Coefficients used in $\tilde{\varepsilon}$ equation

$c_{\varepsilon 1}$	$c_{\varepsilon 2}$	A_d	$c'_{\varepsilon 2}$	$c_{\varepsilon 3}$	$c_{\varepsilon 4}$	$c_{\varepsilon 5}$	c_μ
1.0	$\dfrac{1.92}{1 + 0.7A_d\sqrt{A_2}}$	max(0.2, A)	1.0	1.55	1.0	1.0	0.09

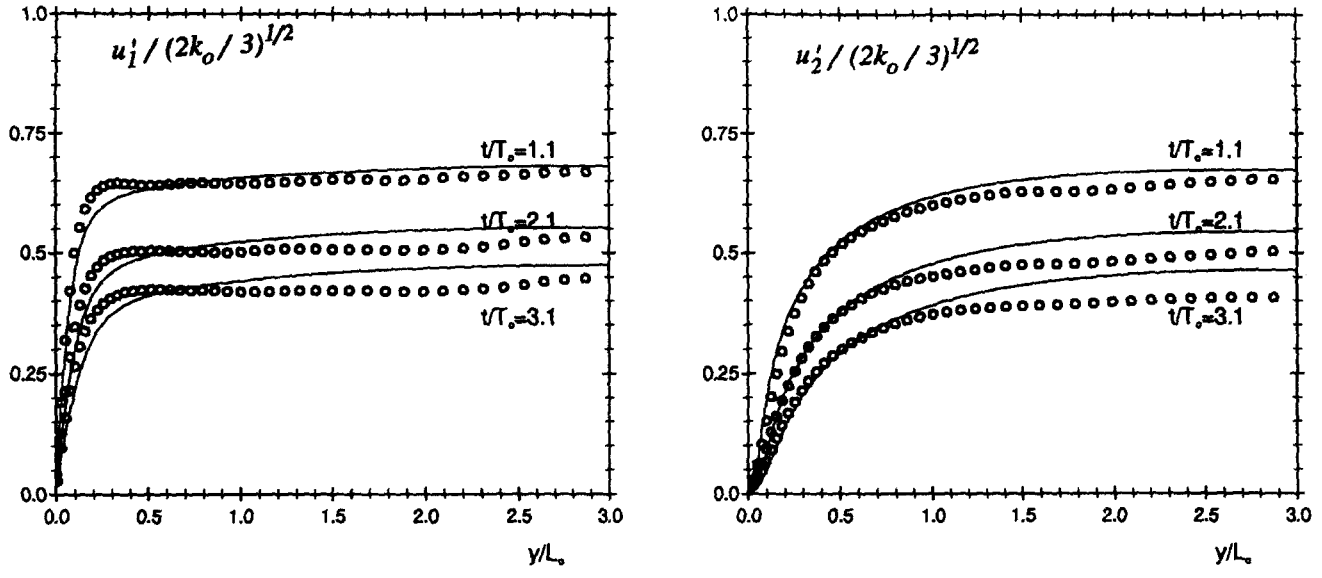

Figure 4 Profiles of u_1' and u_2' in the shear-free wall flow at $t/T_o = 1.1$, 2.1, and 3.1

$$\phi_{ij1}^{\text{inh}} = f_{w1}\frac{\varepsilon}{k}\left(\overline{u_l u_k}d_l d_k\delta_{ij} - \frac{3}{2}\overline{u_i u_k}d_j d_k - \frac{3}{2}\overline{u_j u_k}d_i d_k\right)$$
$$+ f_{w1}'\frac{k^2}{\varepsilon}\left(\overline{u_k u_l}\frac{\partial\sqrt{A}}{\partial x_k}\frac{\partial\sqrt{A}}{\partial x_l}\delta_{ij} - \frac{3}{2}\overline{u_i u_k}\frac{\partial\sqrt{A}}{\partial x_k}\frac{\partial\sqrt{A}}{\partial x_j}\right.$$
$$\left. - \frac{3}{2}\overline{u_j u_k}\frac{\partial\sqrt{A}}{\partial x_k}\frac{\partial\sqrt{A}}{\partial x_i}\right)$$

$$\phi_{ij2}^{\text{inh}} = f_{w2}k\frac{\partial U_l}{\partial x_n}d_l d_n\left(d_i d_j - \frac{1}{3}d_k d_k\delta_{ij}\right)$$

and

$$D_{ij} = -\left(\overline{u_i u_k}\frac{\partial U_k}{\partial x_j} + \overline{u_j u_k}\frac{\partial U_k}{\partial x_i}\right)$$

$$\tilde{\varepsilon} = \varepsilon - 2\nu\left(\partial\sqrt{k}/\partial x_j\right)^2 - \frac{1}{2}f_h\varepsilon_{kk}^*$$

$$c_1 = 3.1f_A'f_{R_t}\min(A_2^{1/2}, 0.5) \qquad c_1' = 1.1 \qquad c_2 = \min(0.55, A^{1.5})$$

$$c_2' = \min(0.6, A^{1.5})$$

$$f_{w1} = 1.9f_{R_t}' \qquad f_{w1}' = 0.22 \qquad f_{w2} = 5f_A$$

$$f_{R_t} = \min(R_t/160, 1) \qquad f_{R_t}' = \min(1, \max(0, 1 - (R_t - 55)/20))$$

$$f_A = \begin{cases} (A/14)^{1/2} & A < 0.05 \\ A/0.7^{1/2} & 0.05 < A < 0.7 \\ A^{1/2} & A > 0.7 \end{cases}$$

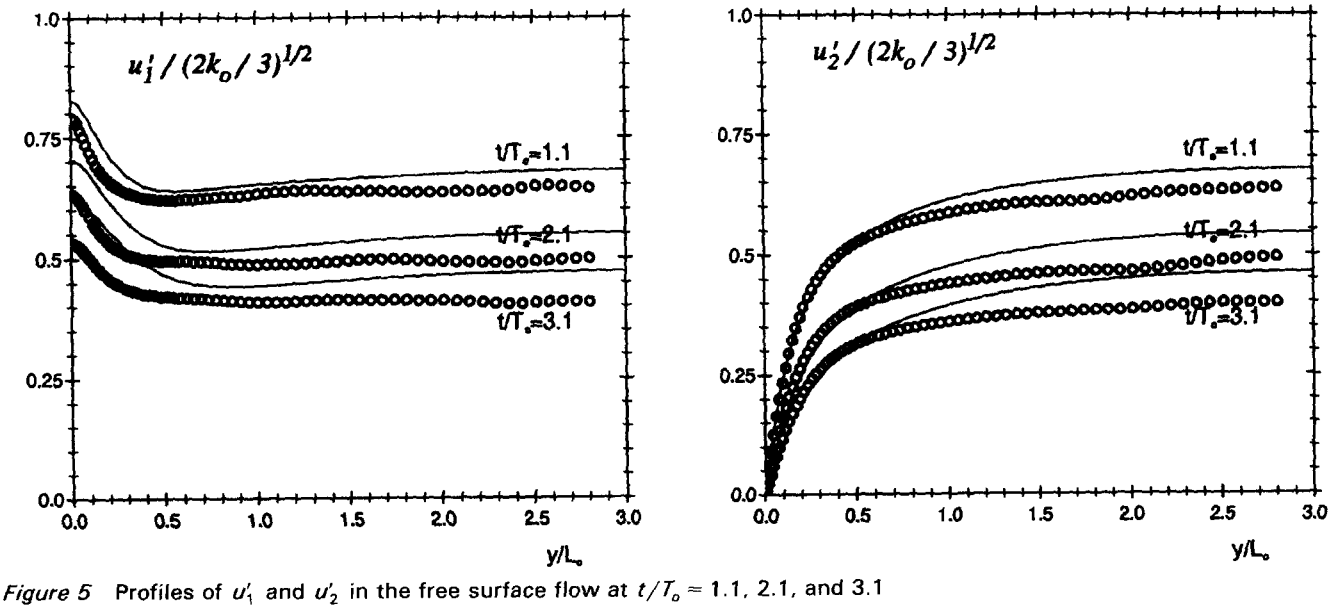

Figure 5 Profiles of u_1' and u_2' in the free surface flow at $t/T_o = 1.1$, 2.1, and 3.1

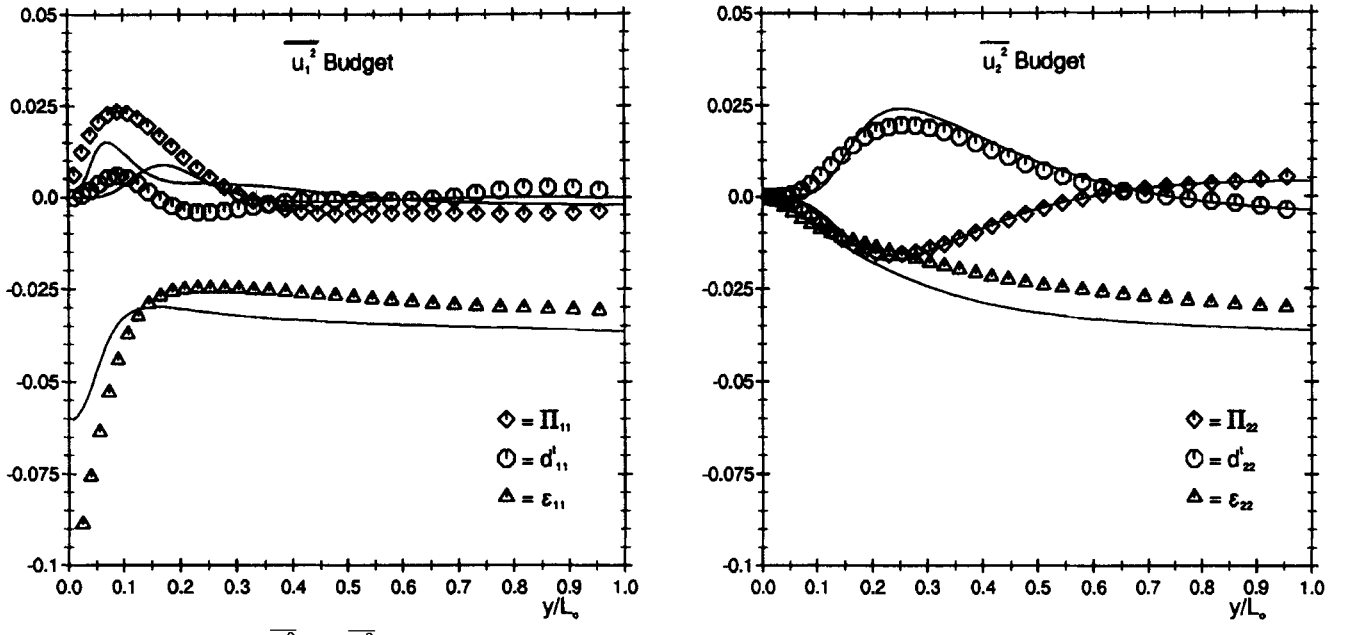

Figure 6 Budgets of $\overline{u_1^2}$ and $\overline{u_2^2}$ in the shear-free wall flow at $t/T_o = 3.1$

The quantities ϕ^*_{ij1} and ϕ^*_{ij2} are based on the high Reynolds number realizable model developed at UMIST. The term ϕ^{inh}_{ij1} can be interpreted as an inhomogeneity correction to ϕ^*_{ij1}, since it involves the length-scale-gradient term d_i, and this has been tuned with reference to the shear-free boundary regions. The ϕ^{inh}_{ij2} correction to the mean-strain-dependent part has a significant effect only in an impinging flow. Further improvements might be brought about by applying an inhomogeneity correction to the velocity gradient along the lines proposed by Launder and Tselipidakis (1993) (see also Launder and Li 1994).

In high-Reynolds-number flows with weak inhomogeneities, the model reverts to the form used previously by the UMIST group to predict a number of free shear flows.

The pressure diffusion term $d^p_{kk} = -(\partial\overline{pu_k}/\partial x_k)/\rho$ also needs modelling, and the present computations have adopted the following interim form

$$\overline{pu_k}/\rho = -(0.5d_k + 1.1d^a_k)(\nu\varepsilon k A A_2)^{1/2} \times [c_{pd1}A_2 + c_{pd2}R_t^{-1/4}\exp(-R_t/40)] \qquad (11)$$

$$c_{pd1} = 1.0 + 2.0\exp(-R_t/40) \qquad c_{pd2} = 0.4$$

which was found to vanish correctly at the wall and to give a reasonable fit to the DNS data.

Dissipation rate equation

The dissipation rate $\tilde{\varepsilon}$ is obtained from the transport equation

$$\frac{D\tilde{\varepsilon}}{Dt} = c_{\varepsilon 1}\frac{\tilde{\varepsilon}P_{kk}}{2k} - c_{\varepsilon 2}\frac{\tilde{\varepsilon}^2}{k} - c'_{\varepsilon 2}\frac{(\varepsilon-\tilde{\varepsilon})\tilde{\varepsilon}}{k} + \frac{\partial}{\partial x_l}\left(\left(\nu\delta_{lk} + c_\varepsilon\overline{u_l u_k}\frac{k}{\varepsilon}\right)\frac{\partial\tilde{\varepsilon}}{\partial x_k}\right) + c_{\varepsilon 3}\nu\overline{u_i u_j}\frac{k}{\varepsilon}\frac{\partial^2 U_k}{\partial x_i\partial x_l}\frac{\partial^2 U_k}{\partial x_j\partial x_l} + c_{\varepsilon 4}\nu\frac{\overline{u_i u_j}}{\varepsilon}\frac{\partial k}{\partial x_i}\frac{\partial U_l}{\partial x_k}\frac{\partial^2 U_l}{\partial x_k\partial x_j} + c_{\varepsilon 5}A^{1/2}(1-A)\frac{\varepsilon}{\sqrt{k}}\overline{u_i u_j}\frac{\partial A}{\partial x_i}\frac{\partial}{\partial x_j}\left(\frac{k^{3/2}A^{1/2}}{\varepsilon}\right) \qquad (12)$$

The terms with coefficients $c_{\varepsilon 1}$, $c_{\varepsilon 2}$, and $c_{\varepsilon 3}$ are standard in appearance (Hanjalić and Launder 1972), though the magnitude of the coefficient $c_{\varepsilon 3}$ is somewhat smaller than in earlier proposals. This reduction in magnitude can be attributed to the inclusion of the term with coefficient $c_{\varepsilon 4}$ which is a generalisation of the proposals of Rodi and Mansour (1993), whilst the final term provides an additional source that is needed at a shear-free boundary. The sink term $(\varepsilon - \tilde{\varepsilon})\tilde{\varepsilon}/k$ acts to give the correct behaviour of $\tilde{\varepsilon}$ very close to the wall. The coefficients take the values given in Table 1.

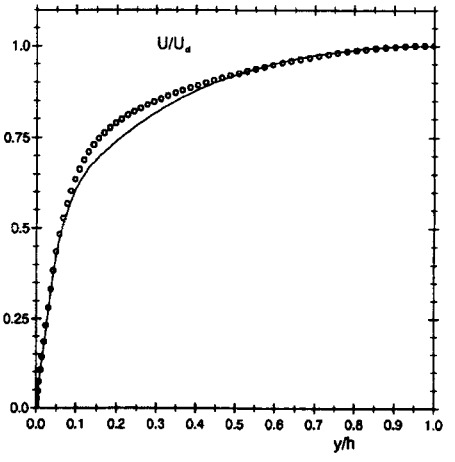

Figure 7 Mean velocity profile in plane channel flow

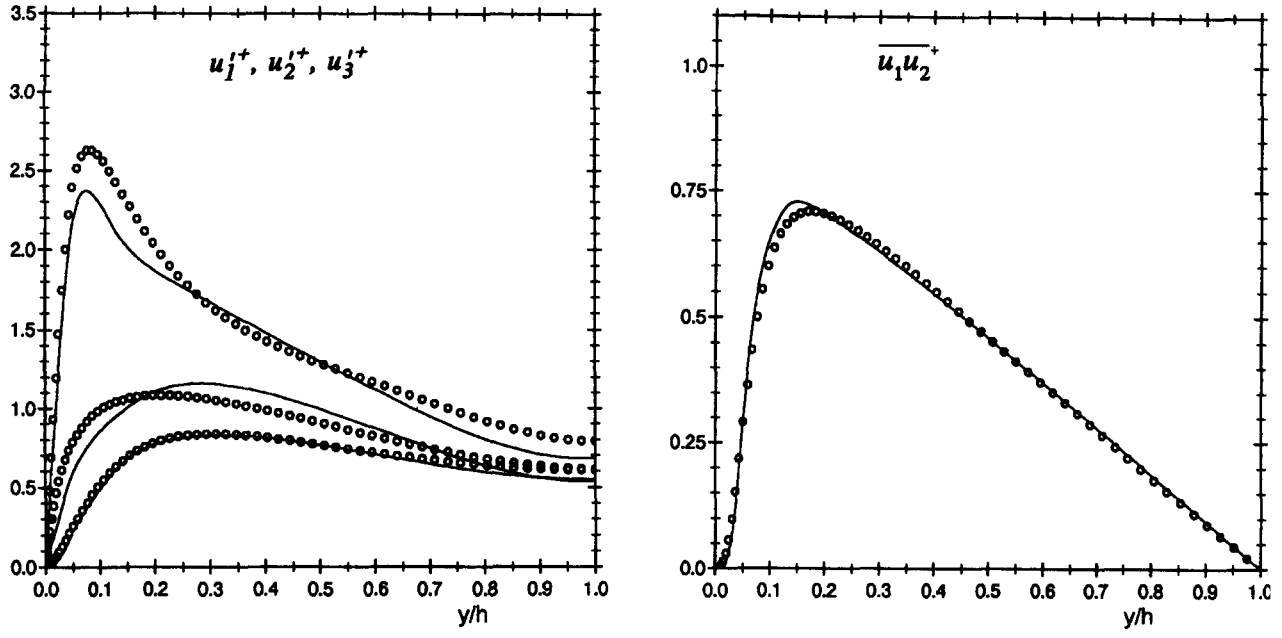

Figure 8 Reynolds stresses in plane channel flow

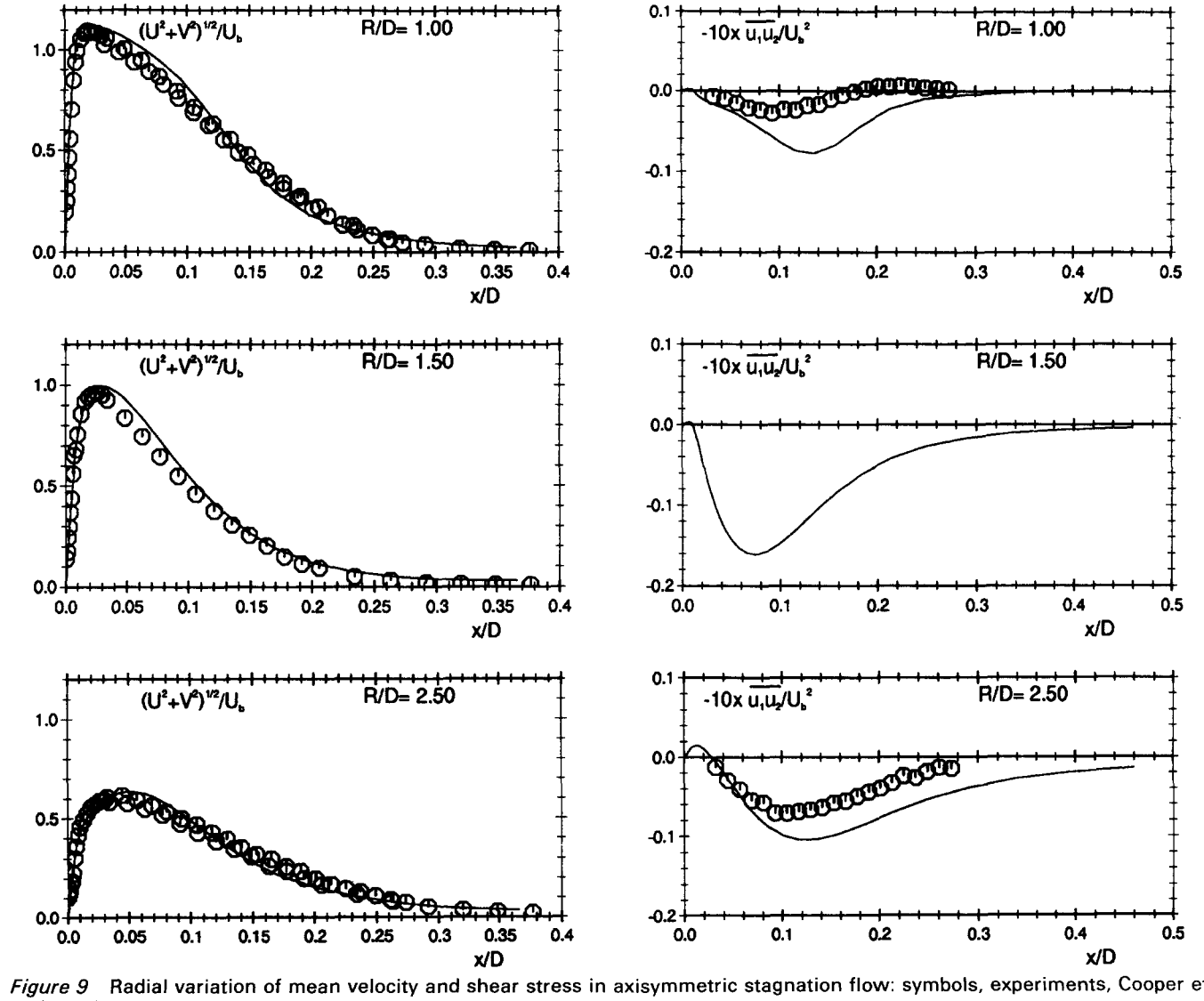

Figure 9 Radial variation of mean velocity and shear stress in axisymmetric stagnation flow: symbols, experiments, Cooper et al. (1993); lines, present computations

Results

Most of the flows have been computed using suitably modified versions of the parabolic code PASSABLE (Leschziner 1982). The shear-free boundary regions are not steady-state flows and were computed by imposing initial conditions corresponding to decaying grid turbulence and then marching the solution through time with the appropriate wall or surface boundary conditions applied. This practice corresponds to the manner in which the DNS data were obtained and allows comparisons to be made at specific times after boundary insertion.

Figure 4 shows the Reynolds normal-stress components perpendicular and parallel to the shear-free wall at three different times after boundary insertion. Corresponding results for the free-surface case are shown in Figure 5. Although the initial effect of the boundary insertion is not particularly well captured, at later times the agreement between computations and DNS improves. While the shear-free wall is well predicted, the free-surface flow shows that improvements are needed close to the surface in order to capture the peak of u_1'. Figure 6 shows elements of the computed budgets of $\overline{u_1^2}$ and $\overline{u_2^2}$ in the shear-free wall case, which are in reasonable agreement with the data.

Figure 7 shows the mean velocity profile for a plane channel flow at a bulk Reynolds number of 5000, while the corresponding shear and normal stresses are shown in Figure 8. The DNS data are from Kim et al. (1987). Although the $\overline{u_2^2}$ profile is well captured, the peak in $\overline{u_1^2}$ is somewhat underpredicted, suggesting that the inhomogeneity correction terms still require some further improvement.

The impinging jet flow provides a very stringent test of any turbulence model, and is a case which many models developed by reference to simple shear flows fail to predict (Craft et al. 1993). The present model has thus been used to compute an axisymmetric jet impinging onto a flat, heated plate from a height of two jet diameters and at a Reynolds number based on jet diameter and bulk velocity of 23,000. Detailed dynamic field measurement for this case have been reported by Cooper et al. (1993), and surface heat transfer measurements have been made by Baughn and Shimizu (1989).

Computations were performed by incorporating the present closure into the elliptic TEAM code, described by Huang and Leschziner (1983). Figure 9 shows mean velocity and shear stress profiles at various radial distances from the stagnation point.

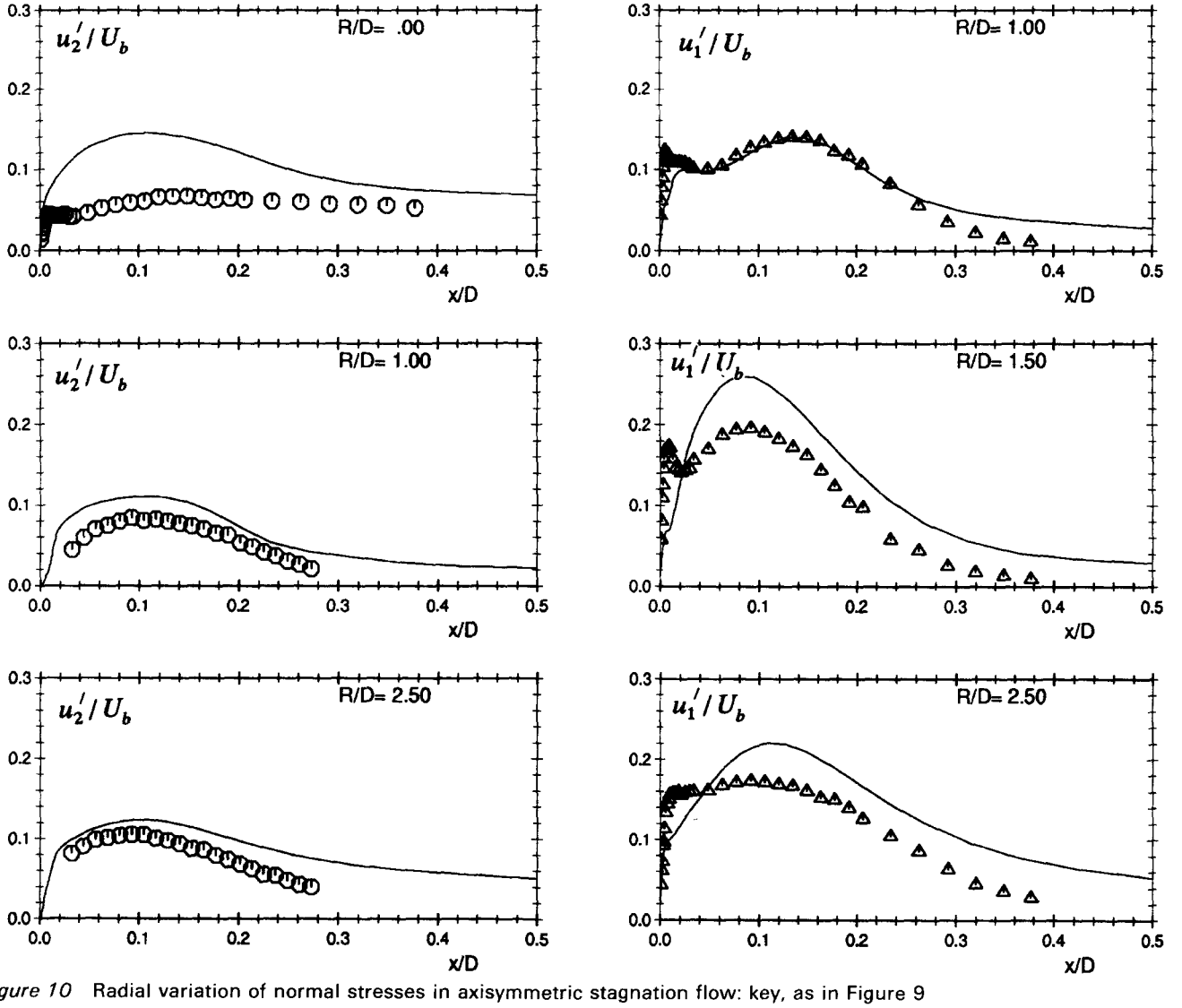

Figure 10 Radial variation of normal stresses in axisymmetric stagnation flow: key, as in Figure 9

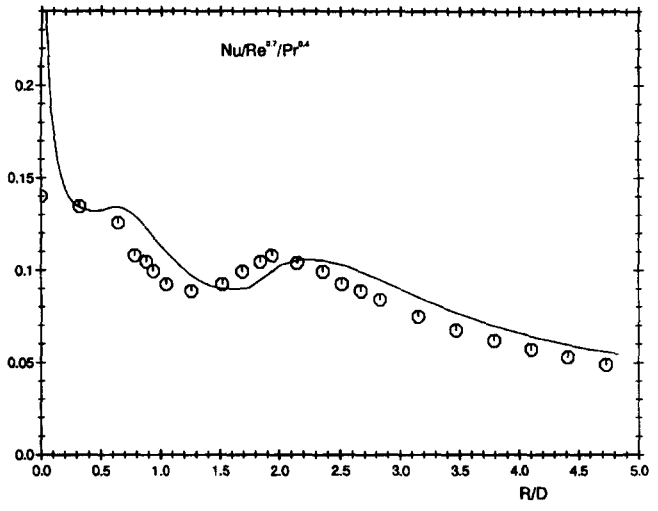

Figure 11 Radial variation of Nusselt number in axisymmetric stagnation flow

While the computed shear stress levels are somewhat too large, this measure of agreement is much better than any earlier second-moment computations that did not explicitly employ wall-distance and normal vectors. The mean velocity-profile comparisons confirm this encouraging trend: the velocity peak *does* decay too rapidly, but the error is fairly modest. Normal stress components parallel and perpendicular to the wall are shown in Figure 10, and are again seen to be in reasonable agreement with the data, although too large levels of $\overline{u_2^2}$ are predicted along the stagnation line.

Finally, Figure 11 shows heat transfer predictions, obtained using the GGDH heat flux model (Daly 1974):

$$\overline{u_i\theta} = -c_\theta \overline{u_i u_j} \frac{k}{\varepsilon} \frac{\partial T}{\partial x_j} \tag{13}$$

with a coefficient $c_\theta = 0.3$. There is clearly a problem at the stagnation point, which would appear to be associated with an overprediction of the turbulent length-scale in this region. At larger radial distances, however, predictions are in better agreement with the measurements, and the shape and position of the secondary peak at around $R/D = 1.5$ are well-captured.

Conclusions

The paper has presented the initial development of a new second-moment closure designed to be applicable over a range of near-wall (and near free-surface) flows without introducing such configuration-specific parameters as wall distance or wall-normal direction (quantities that limit the applicability of any model to simple configurations). The approach has been to extend the realizable free-shear-flow form (that has been in use at UMIST for several years) by introducing markers of the direction of length-scale gradient. These have been used in devising inhomogeneity corrections to the models of pressure-strain and dissipation processes.

While, for flows parallel to walls, the scheme is not yet as successful as the closure of Launder and Li (1994), the new proposals do enable a wider range of near-wall and free-surface flow phenomena to be captured, including the important cases of impinging and shear-free flows. The next steps should be to apply the closure in flows involving successively more complex surface topographies.

Acknowledgment

T. J. Craft acknowledges with gratitude the support of The Royal Society of London through a University Research Fellowship. Authors are listed alphabetically.

References

Baughn, J. W. and Shimizu, S. 1989. *J. Heat Transfer*, **111**, 1096

Cooper, D., Jackson, D. C., Launder, B. E. and Liao, G. X. 1993. *Int. J. Heat Mass Transfer*, **36**, 2675–2684

Craft, T. J., Launder, B. E. and Graham, L. J. W. 1993a. *Int. J. Heat Mass Transfer*, **36**, 2685

Craft, T. J., Launder, B. E. and Leschziner, M. A., 1993b. On the prediction of turbulent flow in spirally fluted tubes. *Proc. 5th Int. Symposium on Refined Flow Modelling and Turbulence Measurements*, Paris

Craft, T. J., Ince, N. Z. and Launder, B. E. 1994. Recent developments in second-moment closure for buoyancy-affected flows. *Proc. 4th Int. Symposium on Stratified Flows*, Grenoble, France

Daly, B. J. 1974. *J. Fluid Mech.*, **64**, 129

Fu, S. 1988. Computational modelling of turbulent swirling flows with second-moment closures. Ph.D. thesis, Faculty of Technology, University of Manchester, Manchester, UK

Hanjalić, K. and Launder, B. E. 1972. *J. Fluid Mech.*, **51**, 301

Huang, P. G. and Leschziner, M. A. 1983. Report TF/83/9, Dept. of Mech. Eng., UMIST

Kim, J., Moin, P., and Moser, R. 1987. *J. Fluid Mech.*, **177**, 133

Kuroda, A. Kasagi, N. and Hirata, M. 1993. Direct numerical simulation of turbulent plane Couette–Poiseuille flows: Effect of mean shear on the near wall turbulence structures. *Proc. 9th Turbulent Shear Flows Symposium*, Kyoto, Japan

Launder, B. E. and Reynolds, W. C. 1983. *Phys. Fluids*, **26**, 1157

Launder, B. E. and Tselepidakis, D. P. 1993. Contribution to the modelling of near-wall turbulence. *Turbulent Shear Flows*, Vol. 8, Springer, Berlin, 81–96

Launder, B. E. and Li, S-P. 1994. *Phys. Fluids*, **6**, 999

Leschziner, M. A., 1982. An introduction and guide to the computer code PASSABLE. Report TF/82/11, Dept. of Mech. Eng., UMIST, Manchester, UK

Lumley, J. L. 1975, *Phys. Fluids*, **18**, 750

Lumley, J. L. 1978, *Adv. Appl. Mech.*, **18**, 123

Perot, J. B. and Moin, P. 1993. Rept. TF-60, Dept. of Mech. Eng., Stanford University, Stanford, CA

Rodi, W. and Mansour, N. 1993. *J. Fluid Mech.*, **250**, 509